Optik - International Journal for Light and Electron Optics 220 (2020) 165185

Contents lists available at ScienceDirect

Optik

journal homepage: www.elsevier.com/locate/ijleo

Original research article

Plasmonic-dielectric hybrid interferometric structures for high-sensitivity refractive index sensing

Rafael Guzman-Cabrera[a], José R. Guzman-Sepulveda[b,*]

[a] Universidad de Guanajuato, Km 3.5 + 1.8 Carretera Salamanca-Valle de Santiago, Salamanca, Guanajuato, 36730, Mexico
[b] Centro de Investigación y de Estudios Avanzados del IPN, Unidad Monterrey. Vía del Conocimiento 201, Parque de Investigación e Innovación Tecnológica, km 9.5 de la Autopista Nueva al Aeropuerto, Apodaca, Nuevo León, 66600 Mexico

ARTICLE INFO

Keywords:
Mach-Zehnder interferometer
Long-range surface plasmon polariton
Optical phase shift
Biosensing

ABSTRACT

In this work, we present a parametric study, by means of numerical simulations, of an integrated Mach-Zehnder interferometer, where the sensing arm consists of a long-range surface plasmon polariton waveguide. Our hybrid dielectric-plasmonic structure is designed specifically for biologically relevant situations, where high-sensitivity sensing of refractive index is critical for tracing small changes in analytes which are commonly presented in aqueous solution form. The design of our device is realistic as it can be fabricated with commercial-grade materials that are commonly available in clean room facilities. Overall, our results validate the use of the proposed structure for high-sensitivity refractive index sensing, based on the sensitivity obtained in our study.

1. Introduction

The high-sensitivity optical sensing of refractive index (RI) requires the use of structures that can respond to small variations in the RI of the sample under study. For this goal, two main approaches are commonly used. The first approach involves the development of optical sensors that are based on extended evanescent fields. These architectures have the ability to report small changes of RI due to the strong interaction resulting from the long extent of the evanescent tails. Typical examples are sensors where longer evanescent tails are generated by tapering optical fibers [1–3] or by using plasmonic configurations [4]. The other approach involves using interferometric detection schemes, which are well known in optics for their large sensitivity. Arguably the most prominent example in biosensing applications is the integrated Mach-Zehnder interferometer (MZI) [5,6]. Just like any other interferometer, sensors based on MZI transform the phase change induced by the variations of RI into a modulated intensity signal which can be useful for sensing.

A hybrid configuration would be highly desirable because two very sensitive elements to monitor RI could be combined: the long-evanescent tails, which are well-known to be sensitive to the waveguide's surroundings, and an interferometric detection which, to this date, is the most sensitive optical measurement of phase changes associated to small RI variations.

Indeed, structures of this nature have been demonstrated based on long-range surface plasmon polaritons (LRSPP) [7], which are transverse magnetic surface waves that propagate on a thin metal slab cladded by dielectrics of similar RI [7,8]. In LRSPP-based sensors, given that the waveguide consists of a thin metal waveguide, the light propagates mostly outside the core thus allowing a strong interaction between the light and the medium surrounding the waveguide.

Based on this concept, all-plasmonic integrated passive optical components have been demonstrated [9,10]. Soon after these

* Corresponding author.
E-mail address: jose.guzmans@cinvestav.mx (J.R. Guzman-Sepulveda).

https://doi.org/10.1016/j.ijleo.2020.165185
Received 14 April 2020; Received in revised form 3 June 2020; Accepted 27 June 2020
0030-4026/

demonstrations, biosensors based on LRSPP waveguides were exploited for a large number of applications, especially by the group of Prof. Berini [11]. Just to name a few examples, biosensors have been developed for the detection of bacteria [12,13] and diagnosis of different diseases [14–17]; others were developed to assess biological affinity [18], to measure biomolecular kinetics [19], and to detect small molecules in general [20]. In all these cases, the sensing principle is based on the modulation of the waveguide's losses by means of small changes in the optical symmetry of the field distribution i.e., the more asymmetric the higher the losses in the waveguide [7,8], which, in turn, results in variations of the transmitted intensity. A common limitation in this approach is the need for long LRSPP waveguides to have enough interaction length, which makes the device susceptible to other detrimental effects such as significant losses due to fabrication defects.

Along similar lines, all-plasmonic integrated interferometers have also been developed for biosensing [21], including interferometers with dual-arm [22] and triple-arm configurations [23,24]. These plasmonic interferometers have a great sensitivity; unfortunately, they share one of the main drawbacks of all-plasmonic optical devices: their inherently higher losses due to the absorption in the metallic portions of the device, which in some cases can constitute the entire structure, and can make them impractical in applications.

In this work, we present the design and numerical simulations of an integrated plasmonic-dielectric hybrid MZI sensor. The sensing arm is a LRSPP waveguide while the rest of the device is all-dielectric and lossless. Moreover, in our device the top cladding of the LRSPP waveguide plays the role of a hypothetical liquid analyte, whose RI index varies around that of water. Our main goal is to assess the feasibility of using this scheme to achieve the high-sensitivity RI sensing required for biosensing. In order to do so, we evaluate the device's performance in conditions of ideal interference, where the arms of the MZI are intensity-balanced. Overall, our results demonstrated the feasibility of using the proposed structure for bio-sensing applications, based on the sensitivity obtained in our study.

2. Structure of the device

We based our design on the vast literature where the design of integrated, dielectric MZI for sensing applications is outlined. In some of those reports, a similar hypothetical situation where the sensing arm of the MZI is covered by a liquid analyte has also been addressed (see, for instance, [25]). We also used our previous results on the characterization of the optical properties of LRSPP waveguides [26]. In general terms, an integrated MZI structure consists of a straight waveguide (input port), which is split by a Y-junction into two arms, which are then recombined by another Y-junction at the end of the active sensing length into another straight

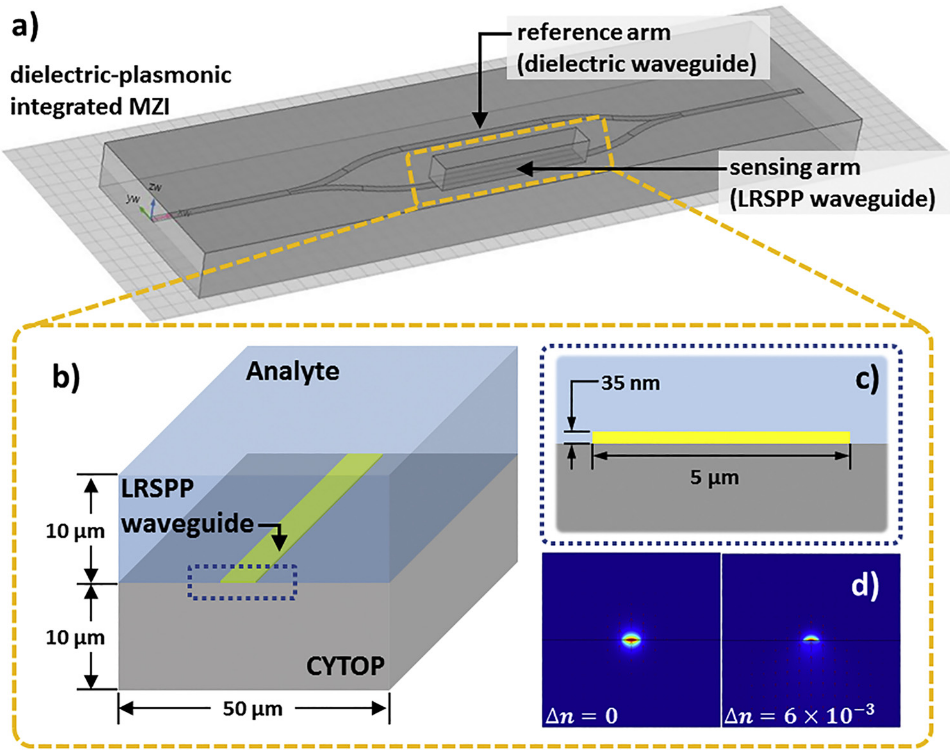

Fig. 1. (a) Schematic of the simulated device, consisting of a LRSPP waveguide incorporated into the sensing arm of an integrated MZI. (b) Zoom-in into the sensing region. The top cladding of the LRSPP waveguide plays the role of a hypothetical aqueous analyte. (c) Dimensions of the LRSPP waveguide. (d) intensity distribution of the optical mode supported by the LRSPP waveguide in the case of symmetric claddings, and for the case when a slight asymmetry is introduced by a small change in the RI of the top cladding, as indicated.

waveguide (output port) [11,25], as shown schematically in Fig. 1(a).

Like any other interferometer, the response of a MZI is based on the difference in the phase accumulated after propagation in both arms. This phase difference, which in turn is produced by the difference between the optical paths in the two arms, translates into a sinusoidal modulation of the light intensity at the output port. Therefore, a MZI can be used as a sensor and its response can be associated to either changes in the physical length of the arms, or changes in their optical properties (arms of equal physical length), or both.

In our configuration, we start from an all-dielectric integrated MZI in which the sensing arm is then replaced by a LRSPP waveguide, in order to enhance the sensing sensitivity, due to the characteristic longer evanescent tails of its supported mode, while maintaining a relatively low attenuation [27].

Fig. 1(b) shows in more detail the region of the sensing arm having the LRSPP waveguide. The waveguide itself consists of a thin stripe of gold (complex RI of 0.55 + i11.4912 at 1550 nm) of thickness 35 nm; see Fig. 1(c). The thickness of the LRSPP waveguide has been strategically chosen in order to balance the sensitivity and the losses [26]. The proposed a design of the device is realistic as can be fabricated in a standard clean room facility with materials commonly available; some important fabrication approaches for similar structure can be found in the literature [9,10].

Given the well-known sensitivity of the LRSPP modes to the optical symmetry of the cladding [7], care should be exerted when selecting the materials. More specifically, in order to make useful RI sensors based on LRSPP modes, one must operate in conditions of slight optical asymmetry for the mode to survive the propagation, and to be able to exploit the large phase accumulated for high-sensitivity sensing.

We envision the proposed device to be useful in biology-related applications, where the samples are typically in aqueous solution form (RI close to that of water (~ 1.33) in the dilute limit [11,20]). Therefore, we chose Cytop as the material for the bottom cladding of the LRSPP waveguide, which has a RI of 1.34 at a wavelength of 1550 nm [28,29]. Basically, in our numerical exercise the top cladding of the LRSPP waveguide plays the role of a hypothetical liquid analyte, which is the typical form of a biological sample (aqueous solution). Therefore, the optical symmetry around the LRSPP waveguide can be mostly preserved when using Cytop in the bottom cladding.

For simplicity of the design, Cytop is also considered as the material for the cladding in the rest of the MZI. In the dielectric portions of the MZI, we consider the core of the waveguides to be made of the commonly used SU-8 photoresist (RI of 1.575 at 1550 nm [25]), which allows ensuring total internal reflection and a good confinement in the dielectric waveguides.

Our numerical study was carried out using the COMSOL Multiphysics software [30]. Our simulations focused on conditions of slight optical asymmetry ($n_2 \approx n_1$) where small variations in the RI of the top cladding are reflected in the complex effective RI of the LRSPP mode. As an example, Fig. 1(d) shows the field intensity distribution of the mode supported by the LRSPP waveguide, for the case of symmetric claddings ($\Delta n = 0$) and for the case when a small asymmetry, $\Delta n = 6 \times 10^{-3}$, is introduced.

The total simulation area is a rectangular region of 50 μm × 20 μm (Fig. 1(b)). A region of these dimensions is enough to provide accurate results with negligible influence of the boundaries. The simulations were performed using a personal computer (Intel i7; 2.59 GHz;16GB of RAM) and in all cases the number of finite elements was at least 1×10^5. The main outcome of our simulations is the complex effective RI, $\eta_{eff} = n_{eff} + ik_{eff}$, of the LRSPP mode supported by the metallic waveguide. As it is natural in a finite-element methodology, spurious solutions arise, especially when an inappropriate initial guess is given or when one is searching for higher-order modes. In our case, the identification of the valid solutions was straightforward due to the set of unique features that make the LRSPP mode clearly distinguishable [7]: the TM-like (vertical) polarization of the associated field distribution; a large electric field concentration near the waveguide; evanescent tails which decay in a way close to a negative exponential; and a complex propagation constant, or equivalently a complex effective RI, with small imaginary part and whose real part is close to that of the dielectric cladding.

3. Results

As mentioned before, the interference between the signal in the reference arm and the sensing arm is practically modulated by the difference in the optical path between the two arms. Given that in our configuration both arms have the same physical length, L, the phase difference is determined only by the difference in the effective RI of the propagating optical modes, [11,25]:

$$\Delta\varphi = \frac{2\pi L}{\lambda}(n_{eff,r} - n_{eff,s}) \tag{1}$$

where $n_{eff,r}$ is the effective RI of the optical mode supported by the dielectric waveguide in the reference arm, and $n_{eff,s}$ is the real part of the effective RI of the optical mode supported by the plasmonic waveguide in the sensing arm.

The characteristic propagation length of an LRSPP waveguide with a thickness of ~35 nm can be slightly longer than 2 mm [26]. At the same time, it is desired that the active sensing length is as long as possible. Therefore, in this work we use a MZI whose arms have length of $L = 2\,mm$, which allows maximizing the interaction distance for sensing without inducing significant losses. This parameter is kept fixed throughout our simulations.

We verified that the optical mode supported in the reference arm (SU-8 embedded in a matrix of Cytop) has $n_{eff,r} = 1.3397$, and its associated amplitude field distribution is symmetric due to the top and bottom claddings have the same RI.

Finally, at the output port of the integrated MZI waveguide, the intensity resulting from the combination of the electromagnetic waves that propagated through the arms of the MZI can be detected. The output intensity is characterized by being changed by the phase difference between the reference arm and the sensing arm [25]. The normalized output intensity can be represented simply as:

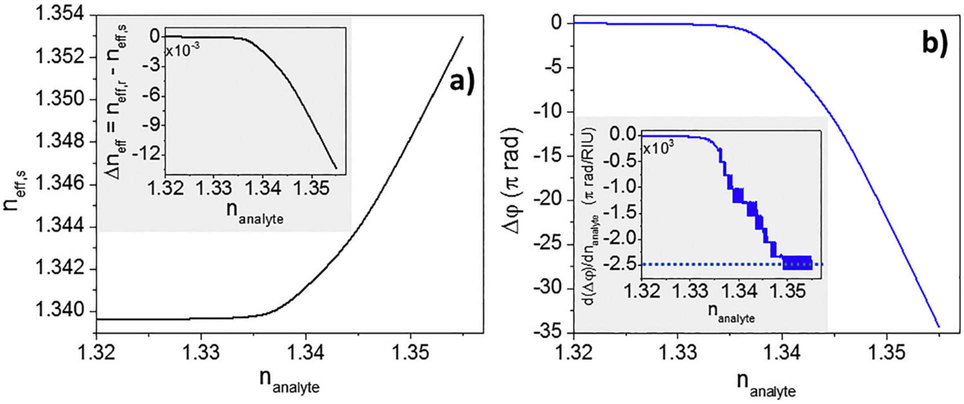

Fig. 2. (a) Effective RI of the LRSPP mode, n_{effs}, as a function of the RI of the analyte, $n_{analyte}$. The inset shows the difference with respect to the reference arms, $\Delta n_{eff} = n_{eff,r} - n_{eff,s}$. (b) The corresponding phase difference, $\Delta\varphi$, calculated using Eq. (1), for an operating wavelength of 1.55 μm and a length of the arms in the MZI of L = 2 mm. The inset shows the derivative (local slope) of the curve in the main plot, which is a direct measure of the sensitivity of the device. From this plot, a huge sensitivity can be expected due to the large values of $\Delta\varphi$ induced with a small change in $n_{analyte}$ (see text for details).

$$I = \frac{1}{2}(1 + \cos(\Delta\varphi)) \tag{2}$$

which represents the case of ideal interference, where the two arms of the interferometer are assumed to have balanced intensity thus providing an interference signal with the largest possible contrast i.e., unitary visibility. We opted for this approach to provide a first-order estimation of the sensing capabilities of the proposed structure.

We explored a RI range of the top cladding, $n_{analyte}$, from 1.320 to 1.355, in steps of 1×10^{-4}. Strictly speaking, changes in $n_{analyte}$ affect the complex effective RI of the LRSPP, $n_{LRSPP} = n_{eff} + ik_{eff}$ [26]. In fact, based on this idea, the straight LRSPP waveguide alone can be actually used as a sensor that is based on the attenuation $\alpha = k_{eff} k_0$ produced by the change in the RI in the top cladding [11].

Nevertheless, by incorporating a LRSPP straight waveguide into a MZI configuration, our interest focuses mainly on the real part of the effective RI of the plasmon mode (this is what induces the phase difference in the interference), which turns out to be the effective RI of the sensing arm $n_{eff} = n_{eff,s}$. Therefore, our simulation strategy consists basically on the numerical calculation of $n_{eff,s}$ as function of $n_{analyte}$; then, we calculated the corresponding phase difference, using Eq. (1); and, finally, we obtained the modulated intensity at the output of the MZI, using Eq. (2).

Fig. 2(a) shows how $n_{eff,s}$ changes with $n_{analyte}$. The inset shows the difference with respect to the reference arm, $\Delta n_{eff} = n_{eff,r} - n_{eff,s}$.

Fig. 2(b) shows the corresponding phase difference, $\Delta\varphi$, calculated using Eq. (1). The inset shows the derivative of the curve in the main plot, which is a direct measure of the sensitivity of the device. This is precisely the hallmark of the combination of an interferometer and a plasmonic structure with long evanescent tails: its extremely large response. In fact, it has been recently demonstrated that such characteristic can be advantageous for the construction of highly integrated devices where a massive phase modulation can be achieved [31].

In our case, the maximum change in the phase difference that can be achieved is of about 2.5×10^3 (πrad)/RIU (see Fig. 2(b)). This means that a small change $n_{analyte}$ of only 4×10^{-4} will be sufficient to induce a change in the phase difference of π rad, which would cover basically the entire dynamic range of the interferometer.

Fig. 3 shows the intensity distribution of the mode supported by the LRSPP waveguide, for the values of $n_{analyte}$ indicated. For cases when $n_{analyte} < n_{Cytop}$ most of the field is at the bottom cladding, outside the waveguide (see Fig. 3(a)). As the difference between the RI of the bottom and top claddings decreases, the intensity distribution becomes more symmetric and most of the field is around the core (see Fig. 3(b)). Finally, when $n_{Analyte} > n_{Cytop}$ most of the field is again outside the waveguide, this time displaced towards the detection window (see Fig. 3(c)).

Fig. 4(a) shows the normalized output of the MZI, calculated using Eq. (2), for the RI range of interest. From Fig. 4(a), two important features can be analyzed, as indicated. First, a measure of sensitivity can be extracted from the local slope at the points of half-intensity; at these points, the largest change of intensity per unit of RI is obtained. Also, the dynamic range for an unambiguous measurement is given by the separation between adjacent maxima in the fringe pattern. Fig. 4(b) shows a plot of these two parameters; we estimated the local slope at all the half-amplitude crossing points, and the RI separation for all the pairs of adjacent maxima.

Fig. 4(b) illustrates the compromise for RI sensing between the dynamic range of the measurement and the sensitivity at which the measurement can be performed: the larger the sensitivity the smaller the dynamic range. In other words, these curves verify that a wide range of RI can be covered only with a low sensitivity; while, on the other hand, if the measurement is performed in a small range of RI, the benefit of a larger sensitivity can be exploited for the measurement. In our case, the largest sensitivity that can be achieved is larger than 3×10^3 RIU^{-1}.

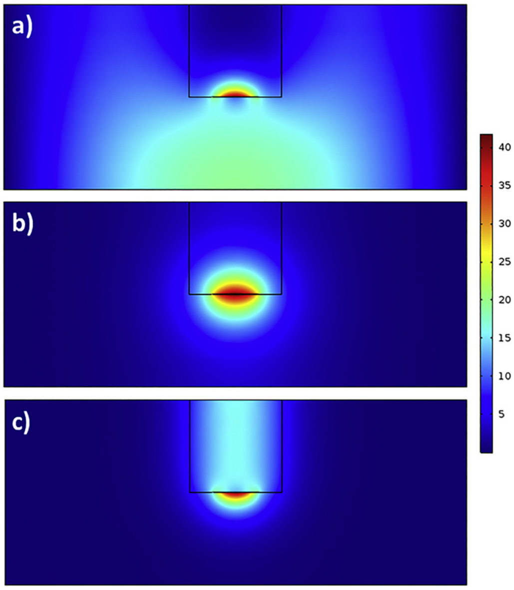

Fig. 3. Electric field amplitude distribution of the optical mode supported by the LRSPP waveguide when the RI of the analyte $n_{Analyte}$ is a) 1.335, b) 1.340, d) 1.345, respectively. The color bar indicates the amplitude of the electric field obtained in the simulations (V/m).

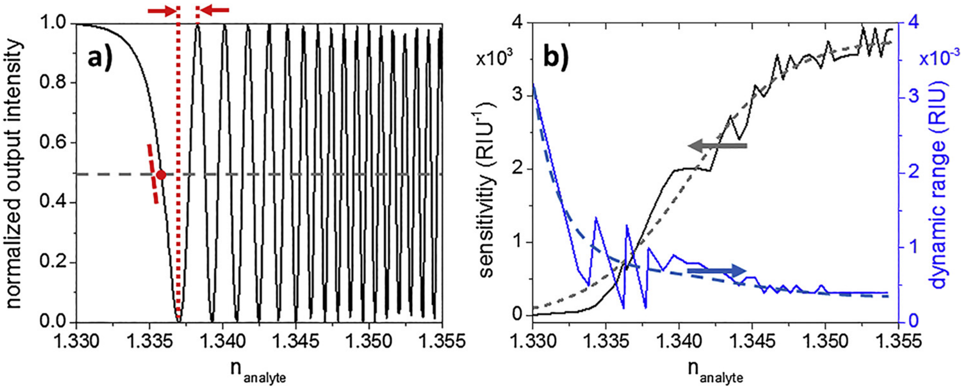

Fig. 4. (a) Normalized output intensity of the MZI. (b) The corresponding sensitivity (local slope at the points of half-intensity; left axis) and the dynamic range for an unambiguous measurement (separation between adjacent maxima in the fringe pattern; right axis).

It is important to note that only in the case of ideal interference, the sensitivity is dictated by the phase difference alone. In real devices the visibility is always smaller than unity and, consequently, the sensitivity is limited i.e., the slope in the interferometer's response is smaller (see Fig. 4(a)). Under these conditions of ideal interference, the sensitivity in our case corresponds to several thousands of dB/RIU, which makes it a good candidate for an "ultra-sensitive" refractometer [4,32].

4. Conclusions and final remarks

We presented a parametric study of an integrated RI sensing platform consisting of an integrated MZI, where one of the arms was replaced by a LRSPP waveguide. In this way, we combine the two more sensitive approaches for RI sensing: a sensing arm with extended evanescent tails for stronger interaction with the device's surroundings, and an interferometric detection scheme.

Our structure is designed specifically for biologically relevant situations, where high-sensitivity sensing of RI in aqueous environments. From a practical perspective, the dielectric-plasmonic hybrid structure proposed has lower losses with respect to all-plasmonic devices since the only metallic portion is the active region for sensing.

Moreover, the design of our device is realistic as it can be fabricated with commercial grade materials that are commonly available in clean room facilities. In this regard, we worked at an operating wavelength of 1.55 μm, not only because it is a standard wavelength for testing integrated devices, but also because it corresponds to a transparency window for the dielectric MZI; however, a similar hybrid structure can be designed for other spectral windows were the absorption of the aqueous samples is also avoided.

From our results, a phase shift of π rad can be induced with a small RI change in the order of 10^{-4}, and a sensitivity larger than 3

$\times 10^3$ RIU^{-1} can be achieved. This makes the proposed structure suitable for biosensing applications.

Finally, in the present work, we addressed the case of ideal interference, where the two arms of the interferometer were assumed to have balanced intensity. Future work will consist on the geometrical optimization of the device, especially the Y-junctions, in order to achieve this.

Declaration of Competing Interest

The authors declare that they have no known competing financial interests or personal relationships that could have appeared to influence the work reported in this paper.

Acknowledgements

The Authors gratefully acknowledge the ETAP Laboratory at the Electrical Engineering Department (DICIS) of the University of Guanajuato, Mexico, for its support with computing resources to carry out the simulations. The Authors are thankful for the constructive comments by the anonymous Reviewers.

References

[1] O.S. Wolfbeis, Fiber-optic chemical sensors and biosensors, Anal. Chem. 74 (12) (2002) 2663–2678.
[2] A. Leung, P.M. Shankar, R. Mutharasan, A review of fiber-optic biosensors, Sens. Actuators B Chem. 125 (2) (2007) 688–703.
[3] J. Wingard, D.L. Wise, Biosensors with fiberoptics, Springer Science & Business Media (2012).
[4] Y. Xu, et al., Optical refractive index sensors with plasmonic and photonic structures: promising and inconvenient truth, Adv. Opt. Mater. 7 (9) (2019) 1801433.
[5] B. Luff, J.S. Wilkinson, J. Piehler, U. Hollenbach, J. Ingenhoff, N. Fabricius, Integrated optical mach-zehnder biosensor, J. Light. Technol. 16 (4) (1998) 583.
[6] M.C. Estevez, M. Alvarez, L.M. Lechuga, Integrated optical devices for lab-on-a-chip biosensing applications, Laser Photon. Rev. 6 (4) (2012) 463–487.
[7] P. Berini, Long-range surface plasmon polaritons, Adv. Opt. Photonics 1 (3) (2009) 484–588.
[8] S.A. Maier, Plasmonics: Fundamentals and Applications, Springer Science & Business Media, 2007.
[9] R. Charbonneau, N. Lahoud, G. Mattiussi, P. Berini, Demonstration of integrated optics elements based on long-ranging surface plasmon polaritons, Opt. Express 13 (3) (2005) 977–984.
[10] R. Charbonneau, et al., Passive integrated optics elements based on long-range surface plasmon polaritons, J. Light. Technol. 24 (1) (2006) 477–494.
[11] O. Krupin, M. Khodami, H. Fan, W.R. Wong, F.R.M. Adikan, P. Berini, Biosensing using long-range surface plasmon waveguides, Integrated Optics: Physics and Simulations III vol. 10242, International Society for Optics and Photonics, 2017, p. 1024203.
[12] M. Vala, S. Etheridge, J. Roach, J. Homola, Long-range surface plasmons for sensitive detection of bacterial analytes, Sens. Actuators B Chem. 139 (1) (2009) 59–63.
[13] P. Béland, O. Krupin, P. Berini, Selective detection of bacteria in urine with a long-range surface plasmon waveguide biosensor, Biomed. Opt. Express 6 (8) (2015) 2908–2922.
[14] W.R. Wong, O. Krupin, S.D. Sekaran, F.R. Mahamd Adikan, P. Berini, Serological diagnosis of dengue infection in blood plasma using long-range surface plasmon waveguides, Anal. Chem. 86 (3) (2014) 1735–1743.
[15] O. Krupin, C. Wang, P. Berini, Detection of leukemia markers using long-range surface plasmon waveguides functionalized with protein G, Lab Chip 15 (21) (2015) 4156–4165.
[16] O. Krupin, W.R. Wong, P. Béland, F.R.M. Adikan, P. Berini, Long-range surface plasmon-polariton waveguide biosensors for disease detection, J. Light. Technol. 34 (20) (2016) 4673–4681.
[17] W.R. Wong, S.D. Sekaran, F.R.M. Adikan, P. Berini, Detection of dengue NS1 antigen using long-range surface plasmon waveguides, Biosens. Bioelectron. 78 (2016) 132–139.
[18] A.W. Wark, H.J. Lee, R.M. Corn, Long-range surface plasmon resonance imaging for bioaffinity sensors, Anal. Chem. 77 (13) (2005) 3904–3907.
[19] M. Khodami, P. Berini, Biomolecular kinetics analysis using long-range surface plasmon waveguides, Sens. Actuators B Chem. 243 (2017) 114–120.
[20] O. Krupin, W.R. Wong, F.R.M. Adikan, P. Berini, Detection of small molecules using long-range surface plasmon polariton waveguides, Ieee J. Sel. Top. Quantum Electron. 23 (2) (2016) 103–112.
[21] D.E. Lee, Y.J. Lee, E. Shin, S.-H. Kwon, Mach-Zehnder interferometer refractive index sensor based on a plasmonic channel waveguide, Sensors 17 (11) (2017) 2584.
[22] H. Fan, P. Berini, Bulk sensing using a long-range surface-plasmon dual-output Mach–Zehnder interferometer, J. Light. Technol. 34 (11) (2016) 2631–2638.
[23] H. Fan, R. Charbonneau, P. Berini, Long-range surface plasmon triple-output Mach-Zehnder interferometers, Opt. Express 22 (4) (2014) 4006–4020.
[24] H. Fan, P. Berini, Bulk sensing using a long-range surface-plasmon triple-output Mach–Zehnder interferometer, Josai Shika Daigaku Kiyo 33 (6) (2016) 1068–1074.
[25] M.R. Ionita, M. Kusko, Design and simulation of a integrated mach-zehnder interferometer sensor, In CAS 2010 Proceedings (International Semiconductor Conference), IEEE, 2010, pp. 529–532 vol. 2.
[26] C.G. Martínez-Arias, M.A. Escobar, J. Guzman-Sepulveda, M. Torres-Cisneros, R. Guzman-Cabrera, Biosensing using long-range surface plasmon structures, in Biosensing and Nanomedicine XI, International Society for Optics and Photonics, 2018, p. 107280F vol. 10728.
[27] C. Chiu, E. Lisicka-Skrzek, R.N. Tait, P. Berini, Fabrication of surface plasmon waveguides and devices in Cytop with integrated microfluidic channels, J. Vac. Sci. Technol. B Nanotechnol. Microelectron. Mater. Process. Meas. Phenom. 28 (4) (2010) 729–735.
[28] G. Khanarian, Optical properties of cyclic olefin copolymers, Opt. Eng. 40 (6) (2001) 1024–1030.
[29] K. Leosson, B. Agnarsson, Integrated biophotonics with CYTOP, Micromachines 3 (no. 1) (2012) 114–125.
[30] COMSOL, Application library manual, Wave Optics Module (2015) COMSOL Multiphysics v5.2.
[31] M. Fuentes-Fuentes, et al., Suspended LRSPP for the development of highly integrated active plasmonic devices, Opt. Express 27 (6) (2019) 8858–8870.
[32] A. Urrutia, I. Del Villar, P. Zubiate, C.R. Zamarreño, A comprehensive review of optical Fiber refractometers: toward a standard comparative criterion, Laser Photon. Rev. 13 (11) (2019) 1900094.